



First Measurement of Collectivity of Coexisting Shapes Based on Type II Shell Evolution: The Case of ^{96}Zr

C. Kremer,¹ S. Aslanidou,¹ S. Bassauer,¹ M. Hilcker,¹ A. Krugmann,¹ P. von Neumann-Cosel,¹
T. Otsuka,^{2,3,4,5} N. Pietralla,¹ V. Yu. Ponomarev,¹ N. Shimizu,³ M. Singer,¹ G. Steinhilber,¹
T. Togashi,³ Y. Tsunoda,³ V. Werner,¹ and M. Zweidinger¹

¹*Institut für Kernphysik, Technische Universität Darmstadt, D-64289 Darmstadt, Germany*

²*Department of Physics, University of Tokyo, Hongo, Bunkyo-ku, Tokyo 113-0033, Japan*

³*Center for Nuclear Study, University of Tokyo, Hongo, Bunkyo-ku, Tokyo 113-0033, Japan*

⁴*National Superconducting Cyclotron Laboratory, Michigan State University, East Lansing, Michigan 48824, USA*

⁵*Instituut voor Kern- en Stralingsfysica, KU Leuven, B-3001 Leuven, Belgium*

(Received 24 June 2016; revised manuscript received 11 August 2016; published 17 October 2016)

Background: Type II shell evolution has recently been identified as a microscopic cause for nuclear shape coexistence. *Purpose:* Establish a low-lying rotational band in ^{96}Zr . *Methods:* High-resolution inelastic electron scattering and a relative analysis of transition strengths are used. *Results:* The $B(E2; 0_1^+ \rightarrow 2_2^+)$ value is measured and electromagnetic decay strengths of the 2_2^+ state are deduced. *Conclusions:* Shape coexistence is established for ^{96}Zr . Type II shell evolution provides a systematic and quantitative mechanism to understand deformation at low excitation energies.

DOI: 10.1103/PhysRevLett.117.172503

Understanding structural changes in nuclei, e.g., the development of coexisting structures with different shapes, is a topic of great interest [1]. In this context the role of the monopole (and quadrupole) parts of the proton-neutron (p - n) interaction has previously been recognized [2]. It has been shown recently that in particular the monopole part of the tensor interaction plays a crucial role for the explanation of shell evolution with varying proton and neutron numbers (type I) [3] as well as for configuration-dependent shell evolution (type II) [4]. While type I shell evolution has been studied extensively, both theoretically and experimentally, cases for type II shell evolution are rare. In particular, data on absolute transition rates for electromagnetic nuclear transitions sensitive to the occurrence of type II shell evolution are still lacking.

Zirconium isotopes show a quick shape phase transition from spherical ground states for $^{90-98}\text{Zr}$ to deformed ground states in ^{100}Zr and heavier isotopes [5]. The nucleus ^{96}Zr has a low-lying excited 0^+ state, which could be deformed, and is suggested as an example for exhibiting type II shell evolution driven by the tensor force. In fact, shape coexistence has been suggested in the heavier isotope ^{98}Zr [1,6] and has recently been reported for the lighter isotope ^{94}Zr [7], albeit a considerable mixing of the coexisting structures was deduced from the sizable interstructure $E2$ transition strengths. To answer the question whether shape coexistence occurs in ^{96}Zr knowledge of electromagnetic transition rates is of utmost importance.

In order to guide the later discussion we briefly review the main points of type II shell evolution due to the tensor force, as presented in Refs. [4,8]. The effect of the monopole part of the tensor force depends on the spin-orbit coupling of the

respective orbitals. In the following we use the standard notation for $j_> = l + s$ and $j_< = l - s$ quantum numbers with spin $s = 1/2$ and orbital angular momentum l . The monopole part of the tensor force is attractive between orbitals with different spin-orbit coupling ($j_> - j'_<$ and $j_< - j'_>$) and repulsive for $j_> - j'_>$ and $j_< - j'_<$ interactions. Thus, a proton excitation from a $j_<$ to a $j_>$ orbital leads to a reduction of spin-orbit splitting for certain neutron orbitals and vice versa (cf. Fig. 1 of Ref. [8]). This leads to an increased likelihood for neutrons to occupy $j'_<$ orbitals, which in turn favors occupation of $j_>$ orbitals for protons. This is a self-reinforcing effect, which can stabilize low-lying deformed configurations (see Refs. [4,8] for more details).

The nucleus ^{96}Zr is a well-suited candidate for featuring type II shell evolution because lifting protons from $p_{1/2}$, $f_{5/2}$ orbitals to the $g_{9/2}$ orbital affects the occupancy of neutron orbitals.

It is the purpose of this Letter to report on an electron scattering experiment off ^{96}Zr , which determines the transition strengths of the 2_2^+ state to low-lying states including the first excited 0_2^+ state. The interpretation of the 0_2^+ state and the band built on top of it as a deformed structure is confirmed, the deformation is deduced, and type II shell evolution is identified as a main stabilizing mechanism of the deformed excited states.

The experiment was conducted at the Superconducting DArmstadt LINear ACcelerator (S-DALINAC) using the Lintott high-resolution magnetic spectrometer [9]. Data were taken at scattering angles of 81° , 93° , 117° , and 141° . An electron energy of 43 MeV was used except for the measurement at 117° , which was performed at

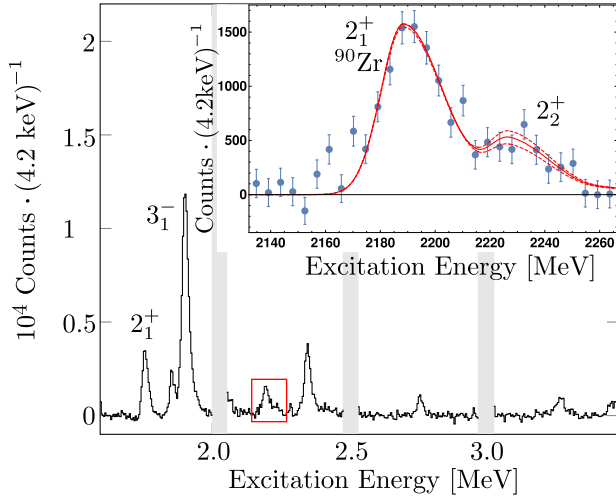


FIG. 1. Summed and efficiency corrected experimental data for $\theta = 141^\circ$ and $E_0 = 43$ MeV after the radiative tail of the elastic line has been subtracted. Gray areas correspond to inactive segments of the detector system. The inlet shows a magnification of the region around the 2_2^+ state of ^{96}Zr , which is indicated by the red rectangle.

$E_0 = 69$ MeV. The covered momentum transfer (q) values were $q = 0.59, 0.40, 0.31,$ and 0.28 fm^{-1} . Intensities of the beam ranged from 0.5 up to 2.5 μA and were limited by the dead time of the data acquisition system [10]. The target used was a 2×3 cm^2 self-supporting zirconium foil of thickness 10 mg/cm^2 . It was enriched in ^{96}Zr up to 57.36% and also contained ^{92}Zr (27.2%), ^{90}Zr (9.2%), ^{94}Zr (4.3%), and ^{91}Zr (2.0%). The resolution of the obtained spectra ranged from 12.3 to 17.5 keV full width at half maximum (FWHM). As an example, the spectrum obtained at 141° is shown in Fig. 1. The $0_1^+ \rightarrow 2_2^+$ transition of ^{96}Zr is located close to the stronger $0_1^+ \rightarrow 2_1^+$ transition of ^{90}Zr with an energy difference of 22 keV only making good resolution critical to the analysis of this experiment as highlighted by the inlet in Fig. 1.

The experimental raw data, consisting of many single runs, were efficiency corrected, energy calibrated, and summed. Then, the elastic background was removed

$$R_F(q) \sqrt{\frac{A_2}{A_1}} \approx \sqrt{\frac{B(E2, k_2)}{B(E2, k_1)}} \left(\frac{1 - \frac{q_2^2}{14} (R_{\text{tr},1} + \Delta R)^2 + \frac{q_2^4}{504} (R_{\text{tr},1} + \Delta R)^4}{1 - \frac{q_1^2}{14} (R_{\text{tr},1})^2 + \frac{q_1^4}{504} (R_{\text{tr},1})^4} \right), \quad (1)$$

where $R_F(q)$ denotes a ratio of kinematical factors [12,13], $R_{\text{tr},1}$ is the transition radius of the 2_1^+ state, $\Delta R = R_{\text{tr},2} - R_{\text{tr},1}$, and k_1 and k_2 denote the photon point momentum transfers for the excitation of 2_1^+ and 2_2^+ states. A χ^2 minimization of Eq. (1) with respect to $T(2_2^+, 2_1^+) = \sqrt{B(E2; 2_2^+ \rightarrow 0_1^+)/B(E2; 2_1^+ \rightarrow 0_1^+)}$ and the difference in transition radii ΔR is carried out. The best fit is represented by the solid red line in Fig. 2 whereas the dashed lines

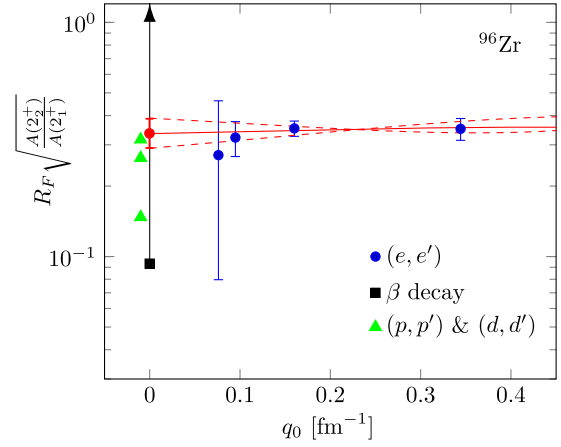


FIG. 2. Value of $R_F \sqrt{A(2_2^+)/A(2_1^+)}$ as a function of elastic momentum transfer q_0 . The solid red line shows the best fit of Eq. (1) to the experimental data (blue circles). The dashed lines represent the 1σ uncertainties with respect to $T(2_2^+, 2_1^+)$. The adopted literature lower limit from β decay [16] is shown as a black square. The green triangles, shifted slightly to the left for readability, represent estimates from (p, p') , (d, d') , and polarized (d, d') measurements [17].

assuming identical line shapes for the peaks corresponding to elastic and inelastic scattering. The number of detected counts A_i for each excited state i can be determined by a χ^2 minimization using an empirical line shape tailored to electron scattering experiments [11]. The extracted peak areas allow us to determine the strength of the $0_1^+ \rightarrow 2_2^+$ transition relative to that of the $0_1^+ \rightarrow 2_1^+$ transition using a plane wave Born approximation (PWBA) [12,13] (cf. Fig. 2). The Coulomb corrections accounting for the distortion of the electron wave functions by the nucleus cancel in this relative analysis to better than 1% over the momentum transfer range of interest. Employing the PWBA formalism using Siegert's theorem and expanding the transition strengths $B(C\lambda, q)$ in powers of the momentum transfer (q) and transition radius (R_{tr}) yields a relation of experimentally determined peak areas to the ratio of $B(E2)$ values

represent the solutions that define the 1σ uncertainties for $T(2_2^+, 2_1^+)$. Using a transition radius $R_{\text{tr},1} = 5.38$ fm, taken from a QRPA calculation, this analysis yields

$$T(2_2^+, 2_1^+) = 0.34_{-0.04}^{+0.05}, \quad \text{and} \\ \Delta R = (-0.22_{-0.92}^{+0.87}) \text{ fm.}$$

The extracted value of ΔR is consistent with zero with an uncertainty of about ± 1 fm. However, the extracted value

TABLE I. Comparison of transition strengths for the low-lying states of ^{96}Zr to the shell-model calculations (SM) and a two-state model with (TSM_m) and without mixing (TSM_u) described in the text. Experimental data obtained in this work are marked by an asterisk (*).

	Experiment	SM	TSM _u	TSM _m
$B(E2; 2_1^+ \rightarrow 0_1^+)$ [W.u.]	2.3(3)	1.28	2.5	2.3
$B(E2; 2_2^+ \rightarrow 0_2^+)$ [W.u.]	36(11)*	52.7	36.7	36
$B(E2; 2_2^+ \rightarrow 0_1^+)$ [W.u.]	0.26(8)*	0.00	0.00	0.26
$B(M1; 2_2^+ \rightarrow 2_1^+)$ [μ_N^2]	0.14(5)*	0.01	0.00	0.07
$B(E3; 3_1^- \rightarrow 0_1^+)$ [W.u.]	57(4)	46.6 ^a
$B(E1; 2_2^+ \rightarrow 3_1^-)$ [W.u.]	$28(9) \times 10^{-3}$ *	0.00

^aEffective $E3$ charges $e_p^{E3} = 1.24e$ and $e_n^{E3} = 0.82e$ are taken by applying $Z = 40$ and $N = 56$ to the estimate shown in Ref. [15].

of $T(2_2^+, 2_1^+)$ is largely independent of the choice of $R_{r,1}$ (at least up to ± 1 fm), see, e.g., Fig. 5 of Ref. [12]. Thus, the data are insensitive to a possible difference of transition radii ΔR of the $0_1^+ \rightarrow 2_{1,2}^+$ transitions (again to about ± 1 fm) indicating that the determination of $T(2_2^+, 2_1^+)$ is independent of ΔR . Combining Eq. (1) with the literature value $B(E2; 2_1^+ \rightarrow 0_1^+) = 2.3 \pm 0.3$ Weisskopf units (W.u.) [14] yields $B(E2; 2_2^+ \rightarrow 0_1^+) = 7.4(2.3) e^2 \text{fm}^4 = 0.26(8)$ W.u. Together with the multipole mixing ratios and the branching ratios taken from Ref. [14] it is then possible to determine all the transition strengths for electromagnetic decays of the 2_2^+ state (see Table I). For the first time our data provide model-independent finite values from an electromagnetic probe for the decay rates of the 2_2^+ state of ^{96}Zr including the $E2$ decay to the 0_2^+ state crucial to determine its structure. The collective value, $B(E2; 2_2^+ \rightarrow 0_2^+) = 36(11)$ W.u., hints at a common deformed structure of the 0_2^+ and 2_2^+ states. Assuming a rigid, axial symmetric, deformed shape the quadrupole deformation parameter β_2 can be estimated

$$\beta_2 = \frac{4\pi}{3ZR_0^2} \left(\frac{B(E2; 0_2^+ \rightarrow 2_2^+)}{e^2} \right)^{\frac{1}{2}} \approx 0.24, \quad (2)$$

where $R_0 = 1.2A^{1/3}$ fm has been used. Thus, the collective $B(E2; 2_2^+ \rightarrow 0_2^+)$ value indicates well deformed 0_2^+ and 2_2^+ states while the weak $B(E2; 2_1^+ \rightarrow 0_1^+)$ strength indicates a nearly spherical ground state for ^{96}Zr .

In light of the experimental data obtained in this work a new shell model calculation for ^{96}Zr has been performed. The model space consists of $1f_{5/2}$, $2p_{3/2}$, $2p_{1/2}$ orbitals, and the full sdg shell for protons and the full sdg shell, plus $1h_{11/2}$, $3p_{3/2}$, and $2f_{7/2}$ orbitals for neutrons. This model space is considerably larger than that of previous shell model calculations (see, e.g., Ref. [18]). Details of the shell model calculation can be found in the preceding Letter [19]. A comparison of transition strengths between low-lying

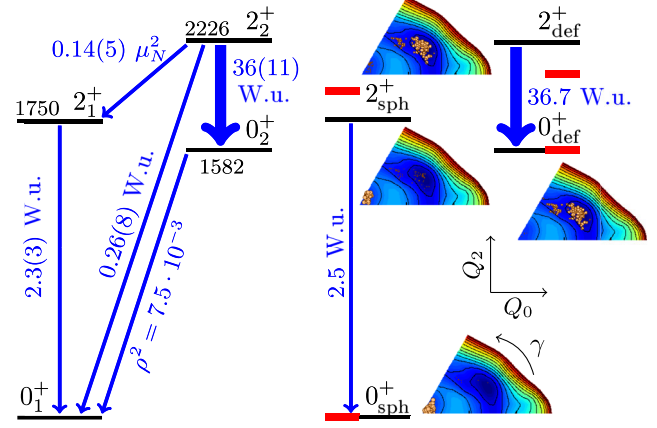


FIG. 3. Low-lying 0^+ and 2^+ states of ^{96}Zr (left) and analyzed underlying structure (right), see text. Experimental excitation energies are given in keV. Excitation energies from the present shell model calculation are indicated by red bars. Note that only the $B(E2; 2_1^+ \rightarrow 0_1^+)$ and $B(E2; 2_2^+ \rightarrow 0_2^+)$ transition strengths have been used in the mixing calculation. The T -plots on the potential energy surface are included, demonstrating different shapes for the ground-state structure (spherical) and for the band on top of the 0_2^+ state (triaxial) (see Ref. [19] for details). The lower left corner of each T -plot corresponds to zero for the quadrupole moments Q_2 and Q_0 . The energy in the contour plot increases from blue (low) to red (high).

states to the experimental values using effective quadrupole charges $e_p = 1.3e$ and $e_n = 0.6e$ is shown in Table I.

The enhanced $2_2^+ \rightarrow 0_2^+$ transition and the small $2_1^+ \rightarrow 0_1^+$ transition strength calculated within the shell model are in qualitative agreement with the experiment. The strong octupole collectivity, a hallmark of ^{96}Zr , is reproduced within 20%. The shell model does not describe the finite $B(M1)$ value between the 2^+ states, which originates from a delicate mixing of the two configurations and hints at a small but finite mixing of the spherical and deformed states.

As both—a deformed and a spherical configuration—coexist at low energies, it is instructive to look at the data in a two-state model (TSM) analysis. Assuming that the experimentally observed states (left-hand side of Fig. 3) are mixtures of deformed and spherical structures, their wave functions can be written as

$$\begin{aligned} |0_1^+\rangle &= \alpha|0_{\text{sph}}^+\rangle + \beta|0_{\text{def}}^+\rangle, \\ |0_2^+\rangle &= -\beta|0_{\text{sph}}^+\rangle + \alpha|0_{\text{def}}^+\rangle, \\ |2_1^+\rangle &= \gamma|2_{\text{sph}}^+\rangle + \delta|2_{\text{def}}^+\rangle, \\ |2_2^+\rangle &= -\delta|2_{\text{sph}}^+\rangle + \gamma|2_{\text{def}}^+\rangle, \end{aligned} \quad (3)$$

where α , β , γ , and δ are amplitudes normalized to $\alpha^2 + \beta^2 = \gamma^2 + \delta^2 = 1$. Using the experimental excitation energies of these states and the observed transition strengths $B(E2; 2_1^+ \rightarrow 0_1^+)$ and $B(E2; 2_2^+ \rightarrow 0_2^+)$ as input data, the mixing amplitudes can be computed under the assumption that the mixing matrix element V_{mix} between

the spherical and deformed structures is identical for the 0^+ and 2^+ states and $E2$ matrix elements between pure configurations vanish. Carrying out the calculation yields

$$\alpha^2 = 99.8\% \quad \beta^2 = 0.2\%,$$

$$\gamma^2 = 97.5\% \quad \delta^2 = 2.5\%.$$

Thus, the states are decoupled to a very good approximation, which is also supported by β decay data [20]. The mixing matrix element amounts to $V_{\text{mix}} = 76$ keV. The interband $B(E2)$ values of the unmixed configurations (right-hand side of Fig. 3) are almost identical to the mixed case.

By measuring the electromagnetic decay properties we have established the high purity of the coexisting states. The present shell model interaction catches the dominant components of the wave functions but is not accurate enough to describing their weak mixing on a percent level. The TSM also provides information on them and hence can be compared to the shell model results. In this case it is justified to interpret the shell model states as an approximation to the pure states of the TSM (cf. right-hand side of Fig. 3). Mixing the shell model states with the deduced mixing matrix element V_{mix} leads to $B(M1; 2_2^+ \rightarrow 2_1^+) \approx 0.07 \mu_N^2$, where the rotational model g factor ($\approx Z/A$) has been used to determine the matrix element $\langle 2_{\text{def}}^+ | M1 | 2_{\text{def}}^+ \rangle$ and the corresponding matrix element of the 2_{sph}^+ state has been calculated using the g factor of the 2_1^+ state ($-0.26 \mu_N^2$) given by the shell model calculation. The resulting $B(M1; 2_2^+ \rightarrow 2_1^+)$ value of $0.07 \mu_N^2$ is reasonably close to the experimental value (Table I), which again suggests that the different shapes coexist with little mixing. This interpretation is reinforced by the clustering of the basis state in the T -plots shown on the right-hand side of Fig. 3 which suggests spherical 0_1^+ and 2_1^+ states and triaxial 0_2^+ and 2_2^+ states (see Ref. [19] for details). An underlying mechanism for stabilizing such coexisting structures has been discussed in terms of type II shell evolution [4,8].

To gain further insight into this mechanism we analyze occupation numbers of single-particle orbitals in the present shell model wave functions shown in Fig. 4. For the ground state of ^{96}Zr all orbitals below the $Z = 40$ and $N = 56$ subshell closures are, to good approximation, filled and those above the subshell closures are empty. The structure of the 2_1^+ state is similar to that apart from one neutron excited from the $2d_{5/2}$ orbital to the $3s_{1/2}$ orbital. The deformed 0_2^+ and 2_2^+ states are also very similar to one another, but markedly different from the spherical states. On average three protons are excited from the pf shell to the $1g_{9/2}$ orbital. In addition, a total of three neutrons are excited from the $2d_{5/2}$ and the $3s_{1/2}$ orbitals to the $2d_{3/2}$, $1g_{7/2}$, and $1h_{11/2}$ orbitals. The large fragmentation of the resulting wave function in terms of spherical shell-model components is indicative of deformation (see Ref. [19] for more details).

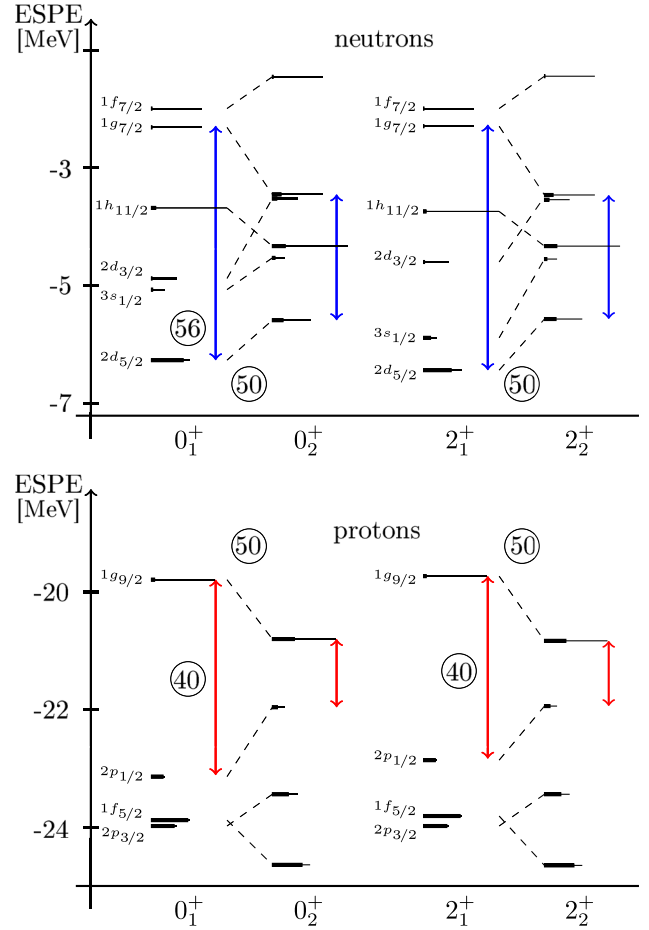


FIG. 4. Effective single-particle energies (ESPE) for neutron (top) and proton (bottom) orbitals of interest to the discussion. The occupation of the orbitals is indicated by thick (filled) and thin (empty) lines. The length of the lines is proportional to the occupation number (thick lines) or the degeneracy of the orbital (thin lines). See text for details.

The difference of occupation numbers between spherical and deformed states (Fig. 4) can be understood in terms of type II shell evolution. For the deformed 0_2^+ and 2_2^+ states the protons in the $1g_{9/2}$ orbital ($j_>$) lead to a reduction of spin-orbit splitting in the neutron sector caused by the monopole part of the tensor force. This effect is enhanced by the fact that the protons are excited to the $1g_{9/2}$ orbital predominantly from $j_<$ orbitals in the pf shell (lower part of Fig. 4). The difference in neutron single-particle energies [19] between the $2d_{5/2}$ and $1g_{7/2}$ orbitals is reduced from 4.0 MeV for the spherical states to 2.1 MeV for the deformed states and is indicated by blue arrows in Fig. 4. Additionally, the neutron single-particle energies of the deformed states are more densely packed around the Fermi energy, which explains the enhanced coherence of various configurations. The increased occupation number of the $\nu(1h_{11/2})$ orbital is due to the central force which outweighs the effect of the tensor force for the interaction of

the $\nu(1h_{11/2})$ - $\pi(1g_{9/2})$ orbitals. In the deformed states the neutrons are more likely to occupy $j_<$ orbitals (e.g., $1g_{7/2}$) than in the spherical states (upper part of Fig. 4). This in turn leads to an increase in spin-orbit splitting in the proton sector. The present shell model calculation shows that the $2p_{1/2}$ - $1g_{9/2}$ gap in the proton effective single-particle energies is lowered from 3.3 MeV in the spherical states ($Z = 40$ subshell closure) to approximately 1.2 MeV in the deformed states as indicated by the red arrows in Fig. 4. Thus, the self-reinforcing effect of type II shell evolution is evident for the SM calculation [19] for ^{96}Zr .

To summarize, electron scattering has been used to measure the $0_1^+ \rightarrow 2_2^+$ transition in ^{96}Zr and determine its strength in a relative PWBA analysis. Using known branching ratios and multipole mixing ratios the electromagnetic decay strengths of the 2_2^+ state have been deduced. The $2_2^+ \rightarrow 0_2^+$ transition strength establishes the 2_2^+ state as a collective excitation on top of a deformed 0_2^+ state with deformation parameter $\beta_2 \approx 0.24$. Type II shell evolution has been proposed as the stabilizing mechanism for the shape coexistence of the low-lying spherical and deformed structures. For the first time, the present experiment provides evidence for the coexisting spherical and deformed structures with little mixing from electromagnetic transition rates.

This work was supported by the Deutsche Forschungsgemeinschaft under Grant No. SFB 1245 and by Grants-in-Aid for Scientific Research (23244049). It was supported in part by the HPCI Strategic Program (hp150224), in part by the MEXT and JICFuS as a priority issue (Elucidation of the fundamental laws and evolution of the universe) to be tackled by using Post “K” Computer (hp160211), and by the CNS-RIKEN joint project for large-scale nuclear structure calculations.

-
- [1] K. Heyde and J. L. Wood, *Rev. Mod. Phys.* **83**, 1467 (2011).
 [2] K. Heyde, P. Van Isacker, R. F. Casten, and J. L. Wood, *Phys. Lett. B* **155**, 303 (1985).

- [3] T. Otsuka, T. Suzuki, R. Fujimoto, H. Grawe, and Y. Akaishi, *Phys. Rev. Lett.* **95**, 232502 (2005).
 [4] Y. Tsunoda, T. Otsuka, N. Shimizu, M. Honma, and Y. Utsuno, *Phys. Rev. C* **89**, 031301 (2014).
 [5] P. Federman and S. Pittel, *Phys. Rev. C* **20**, 820 (1979).
 [6] C. Y. Wu, H. Hua, D. Cline, A. B. Hayes, R. Teng, R. M. Clark, P. Fallon, A. Goergen, A. O. Macchiavelli, and K. Vetter, *Phys. Rev. C* **70**, 064312 (2004).
 [7] A. Chakraborty *et al.*, *Phys. Rev. Lett.* **110**, 022504 (2013).
 [8] T. Otsuka and Y. Tsunoda, *J. Phys. G* **43**, 024009 (2016).
 [9] Th. Walcher, R. Frey, H.-D. Grf, E. Spamer, and H. Theissen, *Nucl. Instrum. Methods* **153**, 17 (1978).
 [10] A. W. Lenhardt, U. Bonnes, O. Burda, P. von Neumann-Cosel, M. Platz, A. Richter, and S. Watzlawik, *Nucl. Instrum. Methods Phys. Res., Sect. A* **562**, 320 (2006).
 [11] F. Hofmann, P. von Neumann-Cosel, F. Neumeyer, C. Rangacharyulu, B. Reitz, A. Richter, G. Schrieder, D. I. Sober, L. W. Fagg, and B. A. Brown, *Phys. Rev. C* **65**, 024311 (2002).
 [12] A. Scheikh Obeid, O. Burda, M. Chernykh, A. Krugmann, P. von Neumann-Cosel, N. Pietralla, I. Poltoratska, V. Y. Ponomarev, and C. Walz, *Phys. Rev. C* **87**, 014337 (2013).
 [13] A. Scheikh Obeid, S. Aslanidou, J. Birkhan, A. Krugmann, P. von Neumann-Cosel, N. Pietralla, I. Poltoratska, and V. Yu. Ponomarev, *Phys. Rev. C* **89**, 037301 (2014).
 [14] D. Abriola and A. A. Sonzogni, *Nucl. Data Sheets* **109**, 2501 (2008).
 [15] A. Bohr and B. R. Mottelson, *Nuclear Structure*, Vol. 2 (Benjamin, New York 1975).
 [16] H. Mach, S. Cwiok, W. Nazarewicz, B. Fogelberg, M. Moszynski, J. Winger, and R. L. Gill, *Phys. Rev. C* **42**, R811 (1990).
 [17] D. Hofer, M. Bisenberger, R. Hertenberger, H. Kader, H. J. Maier, E. Mueller-Zanotti, P. Schiemenz, G. Graw, P. Maier-Komor, and G. Molnar, *Nucl. Phys.* **A551**, 173 (1993).
 [18] K. Sieja, F. Nowacki, K. Langanke, and G. Martinez-Pinedo, *Phys. Rev. C* **79**, 064310 (2009).
 [19] T. Togashi, Y. Tsunoda, T. Otsuka, and N. Shimizu, preceding Letter, *Phys. Rev. Lett.* **117**, 172502 (2016).
 [20] H. Mach, G. Molnar, S. W. Yates, R. L. Gill, A. Aprahamian, and R. A. Meyer, *Phys. Rev. C* **37**, 254 (1988).